X-Band Antenna Gain and System Noise Temperature of 64-Meter Deep Space Stations

B. Benjauthrit and B. D. L. Mulhall
TDA Engineering Office

This report presents a new set of measured data on the X-band performance of the three 64-meter Deep Space Stations. These data will be useful for future mission telecommunication design and predictions. The test configuration and measurement procedure is described. A method of modelling attenuation due to the atmosphere is given. A short review of radio source brightness temperature and flux density is also included.

I. Introduction

The telecommunication design for future missions, specifically in planning for the use of a 64-meter DSS, requires precise knowledge of the system performance of each of the three Deep Space Stations.[1] Only DSS 14 performance had been measured by the Communications Elements Research Section during the X-band cassegrain experimental feedcone development stages; also, by using a noise adding radiometer, data were taken both before (January 1973) and after (May 1973) the antenna modifications (Ref. 1). Additional measurements were made in November 1974 (Ref. 2). Since the other two 64-meter antennas (DSS 43 and DSS 63) are identical in design and construction to DSS 14 before its modifications, their performance specified in the Deep Space Network/Flight Project Interface Design Handbook has been assumed to be approximately the same as that of DSS 14 before antenna modifications.

With the installation of X-band capability at DSS 43 and DSS 63, a measurement program was undertaken to determine their actual X-band performance as part of the continuing effort to upgrade the above mentioned design handbook.

This article describes the test and measurement procedure, the evaluation process, and the data obtained.

II. Test Plan and Radio Sources

Though antenna gain and system noise temperature (T_{OP}) performance curves of DSS 14 are available, in order to verify the previous results and test procedure with the Y-factor technique, the test plan called for new X-band measurements on all three 64-meter stations.

[1] Located at Goldstone, California (DSS 14), Tidbinbilla, Australia (DSS 43) and Madrid, Spain (DSS 63).

To ease the system setup and obtain accurate focussing, strong radio sources were desired. The three chosen non-thermal radio sources were 3C274 (Virgo A), 3C218 (Hydra A), and 3C123. The strength and characteristics of these radio sources at 8415 MHz are given, along with some antenna characteristics, in Table 1 (Refs. 1 and 3). The source 3C274 was the strongest and was used primarily.

III. Test Procedure

The basic principles of the test are as follows: The RF System is calibrated with the antenna at zenith. With the maser on the ambient load, variations in maser gain are recorded on the strip chart as the antenna position is changed. Having completed the maser gain measurements and focussing procedures, the measurement of the RF System parameters by "radio source tracking (by Y-factor)" is started.

A. Measurement of Receiving System Noise Temperature

A simplified X-band receiving system is block-diagrammed in Fig. 1, where:

T_A = effective antenna noise temperature

T_F = effective noise temperature of the components following the maser

T_M = effective travelling wave maser (TWM) noise temperature

T_R = effective receiver noise temperature

= $T_M + T_F$

These effective noise temperatures are all referred to the input to the maser. At stations which have no masers, they are referred to the input to the preamp. Also, all the temperatures are in Kelvins (K) [K = °C + 273.16].

The receiving system may be calibrated by using a noise diode or gas tube (hot load), T_H, a nitrogen cryogenic load, T_N, or a physical ambient load, T_P. The last approach is currently employed.

In the Y-factor technique, the Y-factor is defined by the relationship between the ambient load and the antenna as:

$$Y = \frac{T_P + T_R}{T_A + T_R} \tag{1}$$

Here, T_R is the effective receiver noise temperature and T_A defines the temperature obtained when the receiver is connected to the antenna.

From Fig. 1, the operating system temperature is given by:

$$T_{OP} = T_A + T_R \tag{2}$$

Substituting T_A from Eq. 1 in Eq. 2, and rearranging, yields

$$T_{OP} = \frac{T_P + T_R}{Y} \tag{3}$$

Thus, with T_R known and Y and T_P measured, T_{OP} can be calculated from Eq. (3).

By switching between ambient and cryogenic loads, T_R, if not known, may be determined from the relation:

$$Y_n = \frac{T_P + T_R}{T_N + T_R}$$

where T_N designates the temperature corresponding to cryogenic loads and Y_n designates the corresponding 'y' factor measurement. Note that T_R is usually constant enough that T_M and T_F need not be measured every time it is desired to measure T_{OP}.

A typical noise temperature measurement configuration is shown in Fig. 2. Measurement of the system noise temperature requires the establishment of a noise output level while the receiver input is on the ambient load. The receiver input is then switched to the antenna and the difference in attenuation required to return the receiver to the noise output reference level is then measured, yielding

$$Y = 10^{(A_P - P_A)/10} = ALOG\left(\frac{A_P - A_A}{10}\right)$$

where

A_P = attenuation reading in dB with TWM input connected to the ambient load

A_A = attenuation reading in dB with TWM input connected to the antenna

and $ALOG\ (X)$ denotes the antilog of X.

The Y-factor, together with the other system parameters, is then used in calculating the system noise temperature.

B. Radiometric Technique for Measuring System Efficiency

The radiometric technique for observing radio sources using the *Y*-factor technique is as follows:

(1) Update, if necessary, the focal adjustment setting according to a precalibrated curve. (See Fig. 3 for example.)

(2) Boresight the antenna by using the half-power point method.

(3) Steer the antenna off source (one degree in azimuth if below 45 degrees elevation, one degree in elevation if above 45 degrees elevation). Take attenuation reading (reference).

(4) Steer the antenna on source. Take attenuation reading.

(5) Repeat Step 3.

(6) Repeat Steps 3 through 5 two additional times, alternating the direction of the off-source steering.

Since the system noise temperature varies with time due to elevation angle, as roughly demonstrated in Fig. 4, the procedure described above provides a short and accurate estimate of the performance. This way the operating system temperature for each set of measurements is calculated from:

$$T_{OP}\,(\text{off source}) = \frac{T_{P1} + T_R}{ALOG\left(\frac{A_{P1} - A_{A1}}{10}\right)} \tag{4}$$

The actual source temperature of the first reading is

$$\left.\begin{aligned}\Delta T_{A1} &= T_{OP}\,(\text{on source}) - T_{OP}\,(\text{off source}) \\ &= (T_{P1} + T_R)\left[\frac{1}{ALOG\left(\frac{A_{P1} - \bar{A}_{A1}}{10}\right)} - \frac{1}{ALOG\left(\frac{A_{P1} - A_{A1}}{10}\right)}\right]\end{aligned}\right\} \tag{5}$$

Where $\bar{A}_{A1} = (A'_{A2} + A'_{A1})/2$ is the average of the on-source attenuation's first reading. ΔT_{A2} and ΔT_{A3} can be calculated analogously, noting that $\bar{A}_{A2} = (A'_{A3} + A'_{A2})/2$. The actual source temperature, ΔT_A, is then the average of ΔT_{A1}, ΔT_{A2}, and ΔT_{A3}.

Once the actual antenna system noise temperature is determined, the operating antenna gain can be computed from the relationships:

$$\text{Antenna efficiency} = \eta = \frac{\Delta T_A \cdot C_R}{T_A\ 100\%} \tag{6}$$

$$\text{Antenna gain} = \eta \cdot G_{100\%} = \eta \cdot \frac{4\pi}{\lambda^2} A_p$$

$$= \eta \cdot \left(\frac{\pi D}{\lambda}\right)^2$$

or

$$\text{Antenna gain dB} = 10 \log_{10}\left(\frac{\pi D}{\lambda}\right)^2 + 10 \log_{10} \eta \tag{7}$$

where

$T_A\ 100\%$ = ideal source temperature

A_P = physical antenna aperture area

D = physical diameter of antenna aperture

λ = wavelength of received signal

C_R = resolution correction

$G_{100\%}$ = antenna gain with 100% antenna efficiency

Determination of ideal source temperature is a subject by itself and will not be discussed here. A discussion of the subject may be found in technical description 1008B – "Radio Sources for Antenna Calibrations." The T_A 100% and C_R for 3C123, 3C218, and 3C274 were given in Table 1.

As an example, consider the set of measurements given in Table 2. From this table and Eq. (4), we have

$$T_{OP1}\,(\text{off source}) = \frac{12.60 + 273.16 + 8 + 1.32}{ALOG\left(\frac{52.6 - (44.5 + 44.5)/2}{10}\right)} = 45.702\ \text{K}$$

$$T_{OP1}\,(\text{on source}) = \frac{12.60 + 273.16 + 8 + 1.32}{ALOG\left(\frac{52.6 - 45.94}{10}\right)} = 63.670\ \text{K}$$

$$\therefore \Delta T_{A1} = T_{OP1} \text{ (on source)} - T_{OP1} \text{ (off source)} = 17.968 \text{ K}$$

Similarly, ΔT_{A2} and ΔT_{A3} can be calculated to be 17.980 and 18.366 K, respectively. Thus, the average ΔT_A is 18.108 K and

$$\text{Antenna efficiency} = \frac{18.108}{54.05} \cdot 1.13 = 0.379$$

$$\therefore \text{Antenna gain} = 10 \log \left[\frac{\pi \left(\frac{210}{2} \text{ft} \right)^2 \left(0.305 \frac{\text{m}}{\text{ft}} \right)^2}{(0.0357 \text{ m})^2} \right]$$

$$- 10 \log_{10} (0.379)$$

$$= 10 \log_{10} (3.177 \times 10^7)$$

$$- 10 \log_{10} (0.379)$$

$$= 75.02 - 4.21 = 70.81 \text{ dB}$$

where $C/f = 3.0 \times 10^8 / 8415 \times 10^6 = 0.0357$ m, and C is the speed of light.

IV. Test Results and Discussion

The work to collect data on X-band antenna system noise temperature and gain to verify the data for DSS 14 and to provide actual data for DSS 43 and DSS 63 was undertaken in early September 1976. However, due to bad weather conditions and some anomalies, considerable amounts of early data were discarded. Data considered valid are provided in Figs. 5 through 7.

Figure 3 depicts a precalibrated curve for the antenna focus setting at DSS 14. This curve was obtained by a separate calibration method, which was believed to provide an accurate calibration. This may be observed from the three measured points, obtained during the test on DOY 024 (77).

With the precalibrated focus setting curve in Fig. 3, the system noise temperature vs elevation angle data for DOY 024 (77) and 052 (77) were obtained as shown in Fig. 5a. The solid curve in Fig. 5 and in some later figures was derived from a mathematical model for clear dry weather, with a constant ground temperature. It is used to reflect local ground effects of each station, as well as a reference. (To be discussed further in Section V). The zenith T_{OP} for both days is 27 K. The cloudy condition did not appear to effect the T_{OP} here significantly.

The T_{OP} data from DSS 43 for DOY 024, 040, 045, and 046 (77) are given in Fig. 5b. The lowest T_{OP} is 32 K. The overall T_{OP} is relatively high compared to that of DSS 14 and DSS 63. The discrepancies have not been identified. One possible speculation is that this may be due to ambient load noise causing receiver saturation, making the difference $A_P - A_A$ in Eq. (4) smaller, which results in apparent high measured system temperature. A slight adverse effect of heavy clouds is noticeable in the T_{OP} taken at DSS 63 on DOY 026 and 029 (77), as shown in Fig. 5c. Heavy rain data for DOY 026 (77) are shown in Fig. 5d. The rain started to subside before the data for DOY 026 (77) in Fig. 5c were taken, from 52 deg down. Figure 5e shows the T_{OP} of DSS 63 taken on DOY 037 (77). The lowest T_{OP} for DSS 63 is about 26 K.

Using the derivation described in the last section, the corresponding antenna gain curve for all three stations is given in Fig. 6. Figures 6a and 6b describe the data taken from DSS 14 on DOY 286 (76), 024 (77), and 052 (77). The data are highly packed at elevation angles above 30 deg. The peak gain is about 71.5 dB at 55 deg. Data taken below 30 deg are more scattered, especially at around 8 to 9 deg for DOY 052 (77). This data dispersion is believed to be due to scattering effects at low elevation and the lack of time for precise measurements due to quick rise of the source. Observe that with the same elevation, data from 3C218 appear to scatter more than that from 3C274, a stronger source.

The solid curves A and B are the data from Ref. 1, taken at DSS 14 before and after the antenna modifications, respectively, using the noise adding radiometer technique. They are used here as references.

The new measured data seem to indicate an improvement in gain up to 0.2 dB, compared to the May 1973 curve. No obvious interpretation was noted for this gain improvement, but it is speculated that it was due to the uncertainty of the Y-factor technique.

Figures 6c and 6d depict the gain data obtained from DSS 43 on DOY 321 (76), 024 (77) and DOY 040, 045, 046 (77), respectively. In spite of some dispersion, the majority of the data provides a definite performance pattern. The dispersion is believed to be due to the measurement process. An estimate peak gain is 72 dB at 52 deg. Note that the overall gain curve of the measured data shows an improvement of up to 0.4 dB over the January 1973 curve.

The gain data from DSS 63 are given in Figs. 6e through 6i covering test dates 301, 303, 307 (76) and 026, 029, 037 (77). The data seem to follow the May 1973 curve closely at high elevation angles. It tapers off to the January 1973 curve at low elevation angles. The peak gain is about 71.8 dB at 49 deg.

Note again, that 3C218 offered lower gain and more scattered data than 3C274. A gain performance obtained during a heavy rain is shown in Fig. 6i.

The corresponding curves of antenna efficiency versus elevation angles for all three stations of various test dates are given in Fig. 7.

An estimate of the performance of all three 64-m antenna at X-band are summarized in Table 3.

V. Antenna Performance in the Absence of Atmospheric Losses

The data presented in the previous section include attenuations due to atmosphere, ground, etc. To provide the isolated (in a vacuum) antenna performance, certain attenuation components must be removed from the measured data. To accomplish this, let us first examine the various components of the antenna operating system temperatures. It may be roughly expressed as (see Eq. 2):

$$T_{OP} = T_R + T_A, \text{ K}$$

where

$T_R = T_M + T_F$

$T_A = T_{gnd} + T_{gal} + T_{atm} + T_{\text{hot body}} + T_{ar}$

T_M = effective maser temperature

T_F = effective temperature of components following the maser

T_{gnd} = effective temperature due to spillover and scattering on the ground

T_{gal} = effective galactic temperature

T_{atm} = effective atmospheric temperature

$T_{\text{hot body}}$ = effective temperature of hot body or radio source

T_{ar} = effective temperature of transmission line (coaxial line or waveguide) between antenna and receiver. It is usually small (3.88 K).

The components which give rise to T_{atm} are (see Appendix):

$$T_{atm} = \left[\frac{L_{ox} - 1}{L_{ox}}\right] T_{pox} + \left[\frac{L_{wv} - 1}{L_{wv}}\right] T_{pwv} + \left[\frac{L_{c\ell} - 1}{L_{c\ell}}\right] T_{pc\ell} + \left[\frac{L_{ra} - 1}{L_{ra}}\right] T_{pra}$$

where

$L_{ox}, L_{wv}, L_{c\ell}, L_{ra}$ = losses (in ratio) at a given elevation angle due to oxygen, water vapor, clouds, and rain, respectively.

$T_{pox}, T_{pwr}, T_{pc\ell}, T_{pra}$ = physical temperatures of the respective components

Thus, the total atmospheric attenuation at angle θ, ℓ_θ, is

$$\ell_\theta \text{ (dB)} = (\ell_{ox} + \ell_{wv} + \ell_{c\ell} + \ell_{ra}) \cdot D/a$$

where (for a uniform atmosphere, see Fig. 8)

$D = D_f = a/\sin\theta$, for a flat earth model

$D = D_r = |r \sin\theta \pm \sqrt{(r\sin\theta)^2 + 2ar + a^2}|$, for a round earth model

a = tropospheric thickness, km

r = radio earth radius = 8500 km

$= \frac{4}{3} r_e$, r_e = 6375 km, earth's radius at DSS 14

θ = elevation angle in degrees

$L_{ij} = 10^{\ell_{ij}/10}$, ℓ_{ij} in dB

The flat earth model does not hold at $\theta = 0$ deg, but otherwise provides less than 5.06% error at $\theta \geq 6$ deg (See Table 4)[1]. Thus, the loss in ratio at elevation angle θ, L_θ, is

$$L_\theta = 10^{\ell_z \cdot D/10a}$$

[1] The assumption $r \simeq 4/3(r_e)$ gives a negligibly small error over a more accurate model that is derived from the concept of refractive index, local elevation angles, and a variable absorption coefficient. This model was derived separately by Dr. C. A. Greenhall.

where ℓ_z is the atmospheric loss (in dB) at zenith, and is assumed to be 0.043 dB for clear dry weather.

Most of the parameters given above have been mentioned in previous sections or described in the Appendix. One possible mathematical model is given in Fig. 9,[2] for clear, dry weather (see Appendix). A plot of this mathematical model is given in Fig. 10. Curve 4 was used as a referenced curve in the last section with a constant ground temperature. The value of a is considered to be 10 km here. This is based on the assumption observed from the International Standard Atmosphere (Ref. 4) that air temperature, pressure, and water vapor do not vary appreciably in the region above 10 km, i.e., the influence of the atmosphere above 10 km to T_{OP} is small (see Fig. 11).

There are two possible ways to exclude atmospheric losses from the gain curves given in Section IV. One way is to calculate the losses directly from the recorded weather condition. Another way is to use the clear weather model (Fig. 9) as a basis and then use the difference in the operating system temperatures due to bad weather to calculate the losses due to bad weather. To employ the latter approach, one starts from the equation

$$T_{\theta B} = T_{\theta C} + \Delta T_\theta = \frac{(L_{\theta B} - 1)}{L_{\theta B}} T \tag{8a}$$

or

$$L_{\theta B} = \frac{T}{T - (T_{\theta C} + \Delta T_\theta)} \tag{8b}$$

$$T_{\theta C} = \frac{(L_{\theta C} - 1)}{L_\theta} T \tag{8c}$$

$$L_{\theta C} = 10^{0.0043D} \tag{8d}$$

where

$T_{\theta B}$ = bad weather T_A, K

$T_{\theta C}$ = clear weather T_A, K

$L_{\theta B}$ = bad weather L_θ

$L_{\theta C}$ = clear weather L_θ

ΔT_θ = T_{OP} (bad weather) – T_{OP} (clear weather)

T = weighted average physical temperature of troposphere and r, a, and D were defined previously (see Appendix).

Now let a_{zB} be the loss in dB due to bad weather. Then

$$L_{\theta B} = 10^{a_{zB} D/10a}$$

so that

$$a_{zB} = \frac{10a}{D} \log_{10} L_{\theta B} = \frac{10a}{D} \log_{10} \left[\frac{T}{T - (T_{\theta C} + \Delta T_\theta)} \right] \tag{9}$$

Thus, the gain (in vacuum) performance is obtained by adding the measured gain with the loss $a_{\theta B}$ due to atmosphere. The gain performance plots with atmospheric losses removed for all three stations are given in Fig. 12, a through c.

As an example, consider T_{OP} (bad weather) = 26.83 K, T_{OP} (clear weather) = 26.5 K, $\theta = 90°$, $T = 265$ K. From Eq. (8),

$$L_{\theta C} = 1.00995, \quad T_{\theta C} = 2.61 \text{ K}, \quad \Delta T_\theta = 0.33 \text{ K}$$

so that $L_{\theta B} = 1.011$ and $a_{zB} = 0.048$ dB.

Thus, the atmospheric losses in dB at zenith due to weather is 0.048. Consequently, the loss at elevation angle θ is

$$0.0048 \mid r \sin\theta \pm \sqrt{(r \sin\theta)^2 + 2ra + a^2} \mid /a$$

for the round earth model. Specifically, at $\theta = 30$, the loss is 0.096 dB where $a = 10$ km and $r = 8500$ km.

Figure 13 plots the values of a_{zB} (dB) as a function of $T(K)$ and of $\Delta T_\theta(K)$, using Eq. 9. From the figure, a_{zB} varies only 0.008 dB over 50 kelvins of T, but it changes 0.344 dB over 20 kelvins of ΔT_θ. This establishes that ΔT_θ has more influence on a_{zB} than T, and that the actual value of T is not very critical in determining the atmospheric losses.

VI. Conclusions

Using the Y-factor technique, the new X-band 64-m antenna performance data appear to substantiate the past performance data taken using the noise adding radiometer

[2] Partly proposed by R. Riggs of the Telecommunication Systems Section.

technique, but with some increase in gain for all three stations. The increase in the gain has not been identified but could easily be due to the uncertainty of the Y-factor technique. Further, heavy rains, clouds, and the strength of radio sources were observed to have strong influences on the measurement of performance of the antenna at X-band. Lastly, the overall antenna gain of DSS 14 is observed to be 0.2 to 0.5 dB lower than that of DSS 43 and DSS 63.

Acknowledgment

The authors wish to express their sincere thanks to all parties concerned from the various JPL Engineering Sections and all three 64-m Deep Space Stations in organizing and carrying this effort to a completion. Special thanks are due to R. Caswell who indefatigably collected, analyzed, and turned the data into a useable form. Appreciations are also due to D. Bathker, J. Allen, N. Fanelli, S. Slobin, and A. Caticchio for their special efforts in this regard. In addition, appreciation and acknowledgment are due to A. Freiley for transfer of R&D techniques and experience to operations environment, including major software capabilities.

Table 1. Radio source and 64-m antenna characteristics at 8415 MHz

(a) Radio source characteristics

Characteristic	Radio source		
	3C123	3C218 (Hydra A)	3C274 (Virgo A)
Type	Galaxy	Galaxy	Galaxy
Source shape	Two-dimensional gaussian	Core halo	One-dimensional gaussian
Size, arcsec	20	15 × 45, 200	1 × 45
8415-MHz flux, Janskys[a]	10	8.64	46.3
Spectral index	−0.86	−0.91	−1.02
Position (1950.0)			
Right ascension	$04^h\ 33^m\ 56^s$	$04^h\ 15^m\ 41.5^s$	$12^h\ 28^m\ 18^s$
Declination	29°34′	−11°53′06″	12°40′

(b) 64-m antenna characteristics

Characteristic	Radio source		
	3C123	3C218 (Hydra A)	3C274 (Virgo A)
Antenna polarization	RCP[b]	RCP	RCP
Resolution correction[c], C_R	1.006	1.06	1.13
Antenna temperature[d], T_A, 100%, Kelvins	11.67	10.09	54.05

[a] 1 Jansky = 10^{-26} W m^{-2} Hz^{-1}.

[b] Right circular polarization.

[c] 137 arcsec, half-power beam width selected.

[d] T_A 100% = 1.1674 · source flux (see Eq. A-9).

Table 2. Calculation of antenna performance
(An edited version of the computer printout)

Station	14				
Feedcone	Type XRO; serial number 001; modification 00; polarization 0				
Maser	Serial number XR014				
Receiver	BLK IV, RCV 4				
I.F. attenuator	Serial number lab				
Operator	JE M				
Date (GMT)	Day number 024, year 77, HHMM 545				
Outside weather	Humidity 37 per cent; temperature 8.3°C				
Weather conditions	Clear Clear weather Sun not in beam No R.F. spur No water on horn; answer given: yes				
Radio source	3C-274				
Frequency	8415.0 MHz				
Comments					
Zero ambient load specified for maser ref./gain					
Maser off-on on ambient load	off 28.5 dB; on 52.0 dB				
Maser gain on ambient load	Ref./gain 0.0 dB; maser/gain 45.0 dB				
Ambient load temperature	12.50°C				
Maser gain	45.00 dB; follow on temp. 0.132 ± 01 K				
Maser table constants .. XR014	8395.00	8435.00	8.00	.00	.00
Antenna boresight	Dec or el 0.001 HA or az −0.010				
Block 1					
Offsets, deg	(IF reboresighted)				
Time (GMT), hour: min	06:12				
Antenna elevation angle	9.3 deg				
T_P = Ambient load temperature	12.60°C				
	Y-factor attenuator readings, dB:				
A_A = Antenna off source	44.500	44.500	44.310	44.360	
A'_A = Antenna on source	45.940	45.870	45.850		
A_P = Ambient load	52.600	52.590	52.600		
$T_R = T_M + T_F$ = 8 K + 1.32 K = 9.32 K	T_A 100% = 54.05 K				
Final				Initial average	sigma
Mean sigma antenna system temp.	45.702	44.816	43.998	44.834	.852
Source temp.	17.968	17.980	18.366	18.108	.226
Comments	3C-274				

Table 3. Measured 64-m antenna performance at X-band

64-m DSS	Zenith T_{OP} K (at 86° el)		Peak gain, dB
	Clear dry	Average	
14	26.5	27	71.5 at 55°C
43	27.5	28	72.0 at 52°C
63	24.0	25	71.8 at 49°C

Table 4. Comparison of round and flat earth models for a = 10 km and r = 8500 km

El angle, deg	D_r, km	D_f, km	% error
0	412.43	∞	∞
1	289.95	572.99	97.62
6	91.06	95.67	5.06
30	19.96	20.00	0.20
90	10	10	0

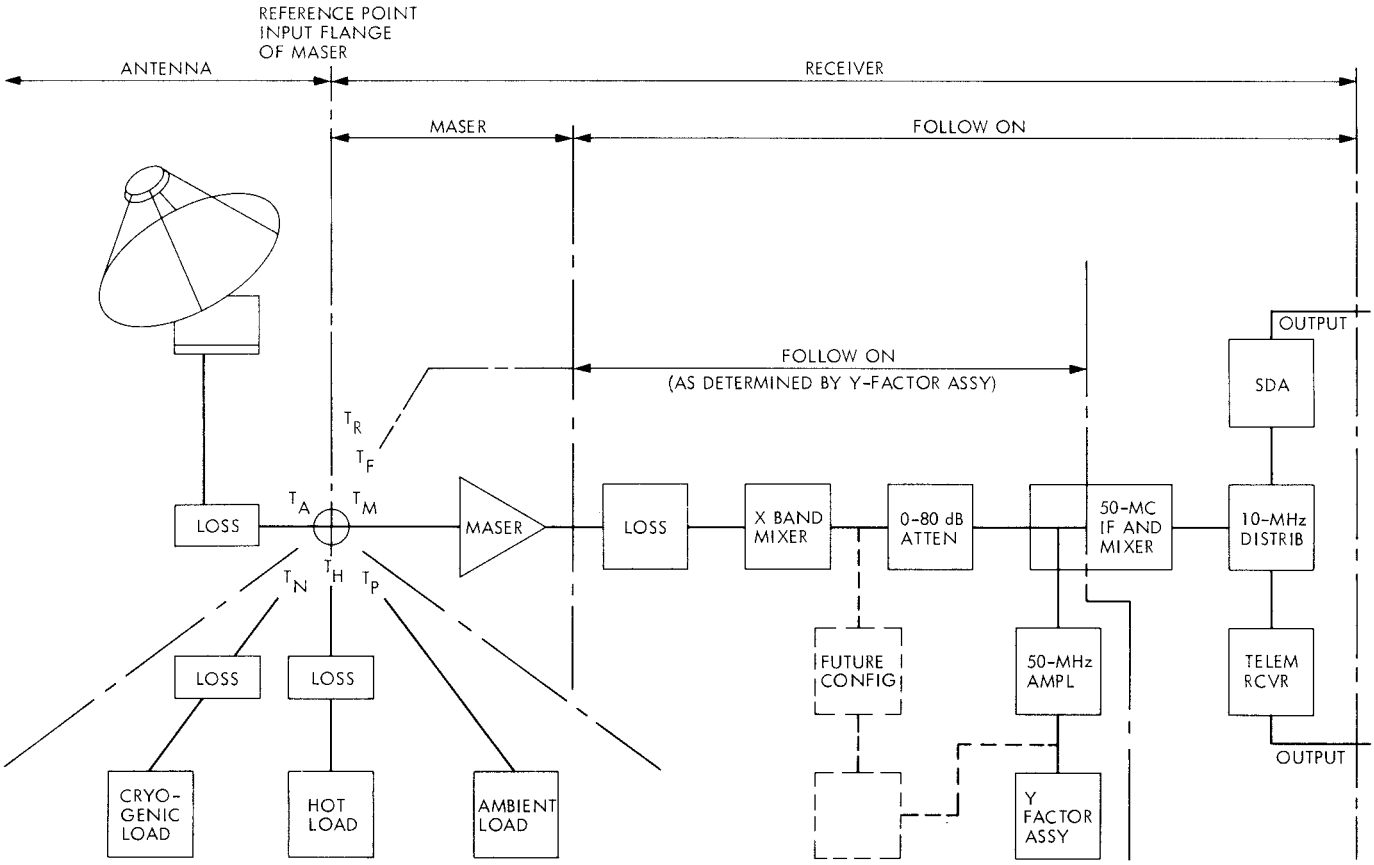

NOTE: CRYOGENIC LOAD AND HOT LOAD ARE NOT GENERALLY AVAILABLE

Fig. 1. Simplified receiving system block diagram

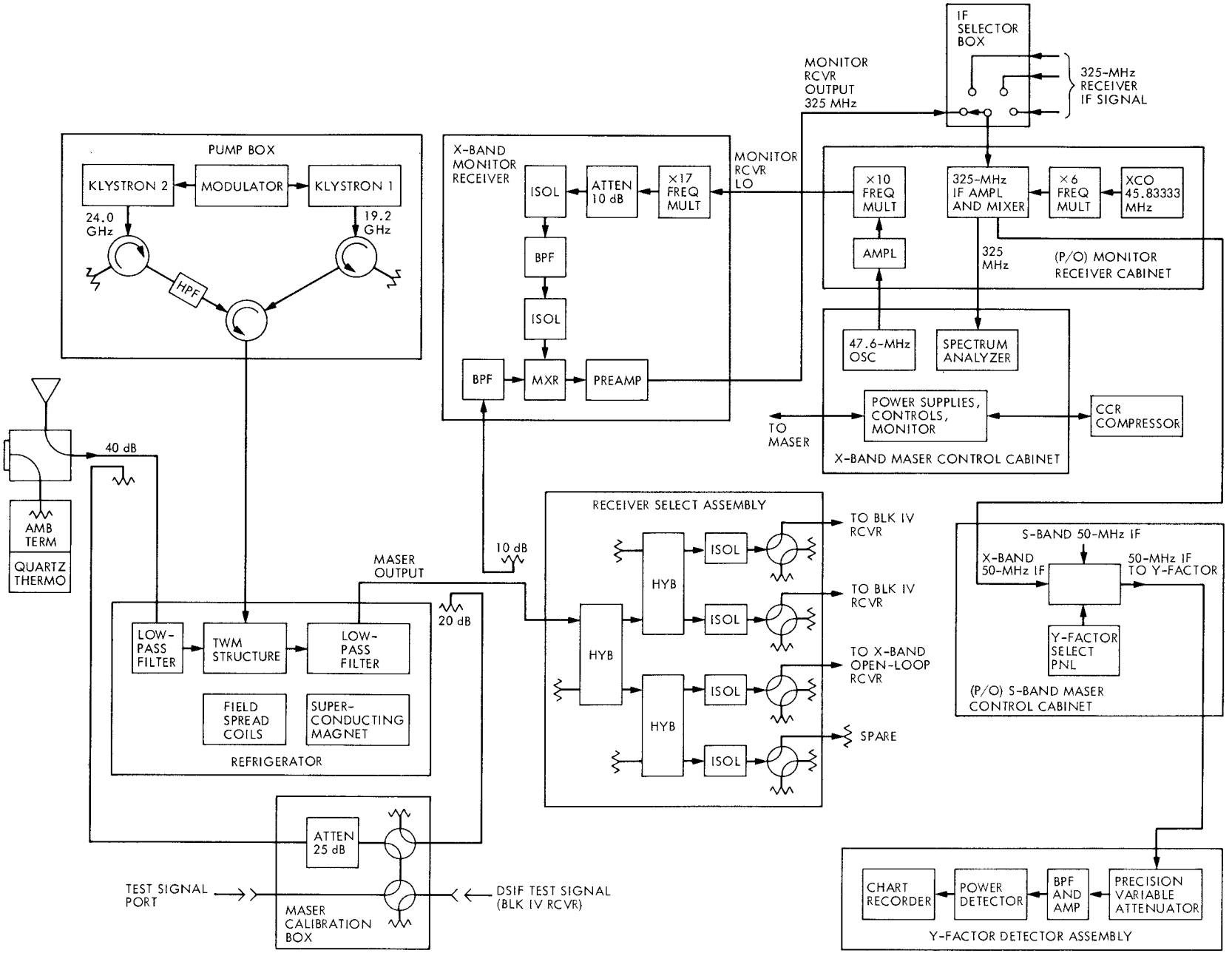

Fig. 2. X-band TWM system noise temperature configuration

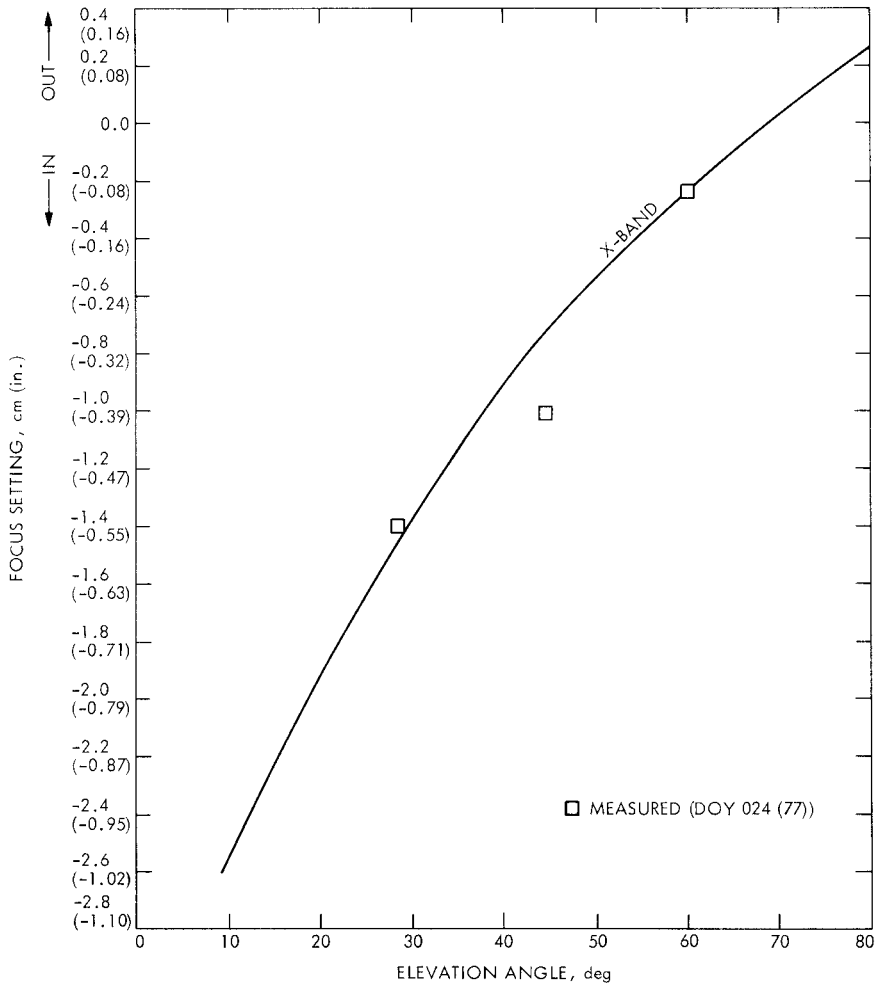

Fig. 3. DSS 14 subreflector axial position at X-band

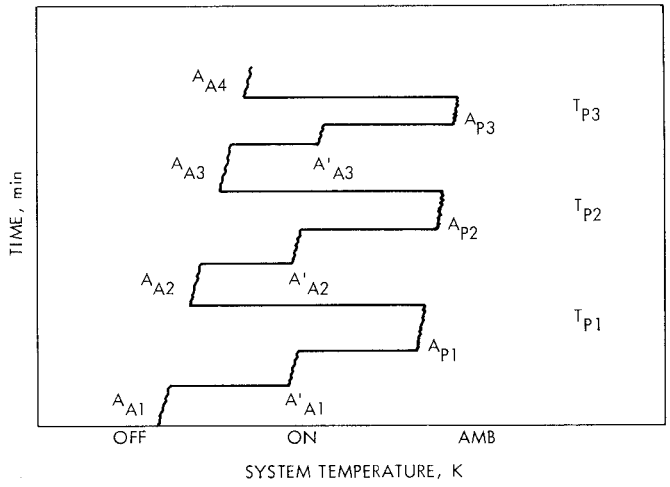

Fig. 4. System temperature varies with time due to elevation angle change

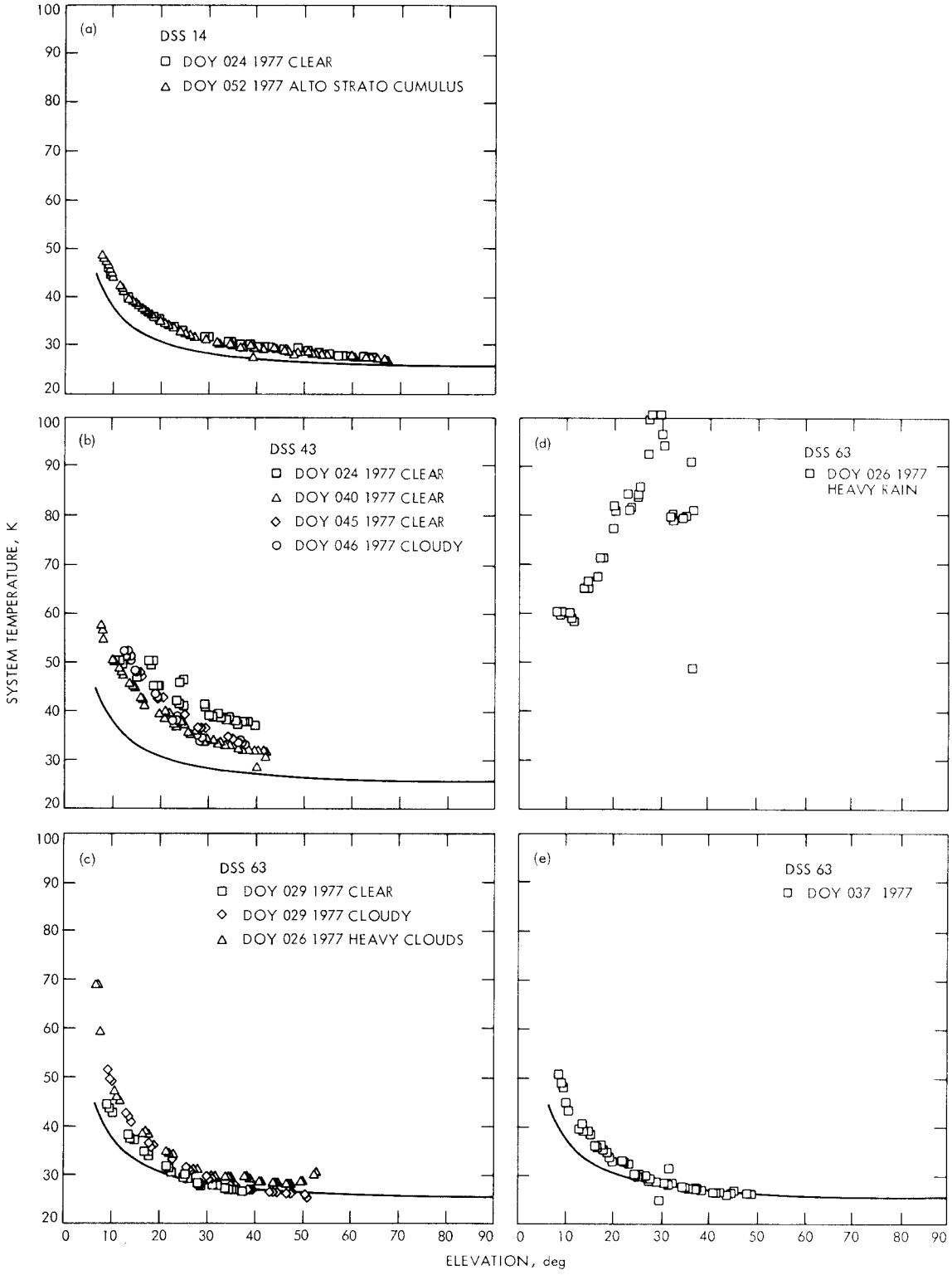

Fig. 5. System noise temperature vs elevation angle at X-band (8415 MHz): (a) DSS 14; (b) DSS 43; (c), (d), and (e) DSS 63

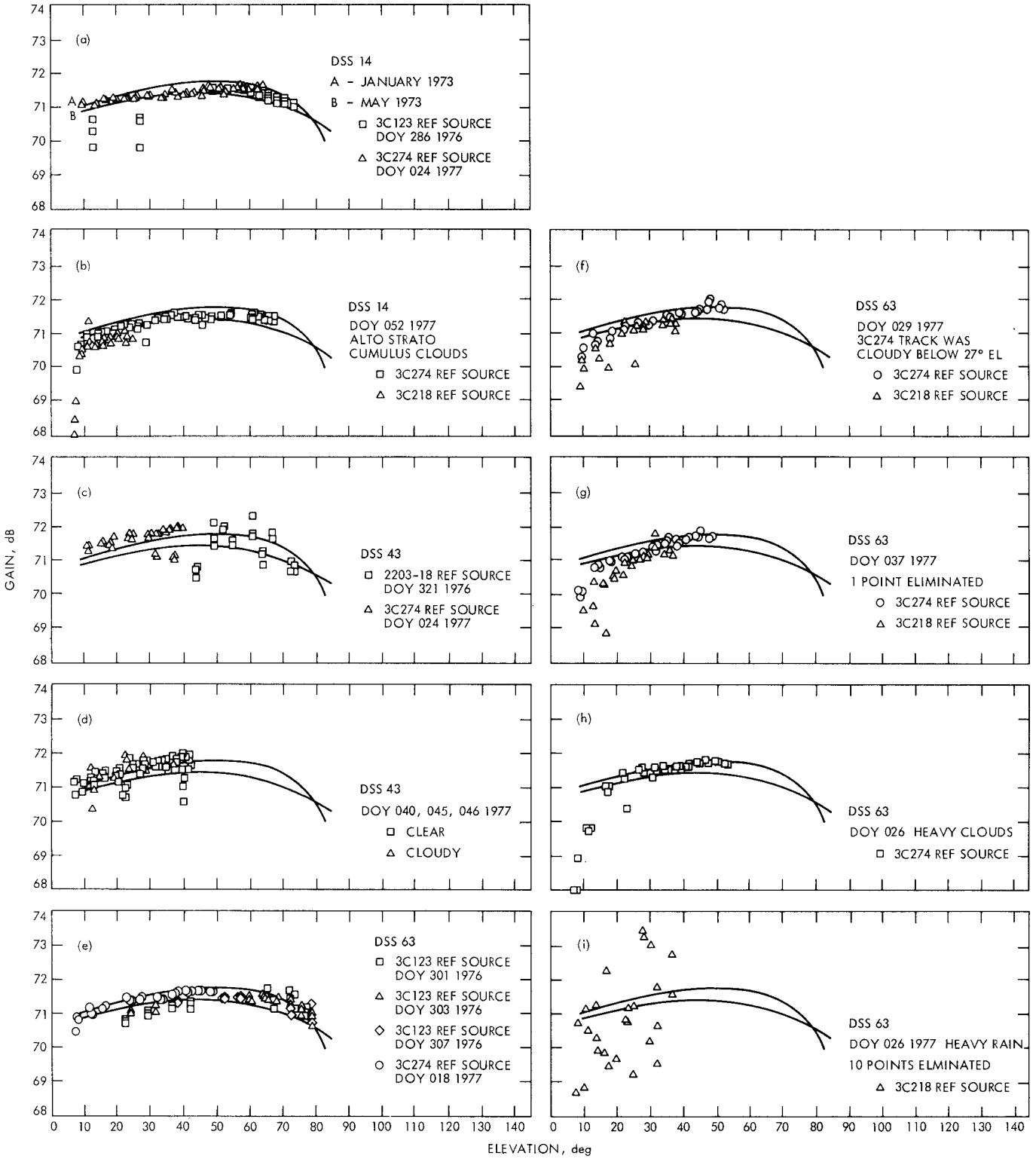

Fig. 6. Antenna gain vs elevation angle at X-band (8415 MHz): (a) and (b) DSS 14; (c) and (d) DSS 43; (e) through (i) DSS 63

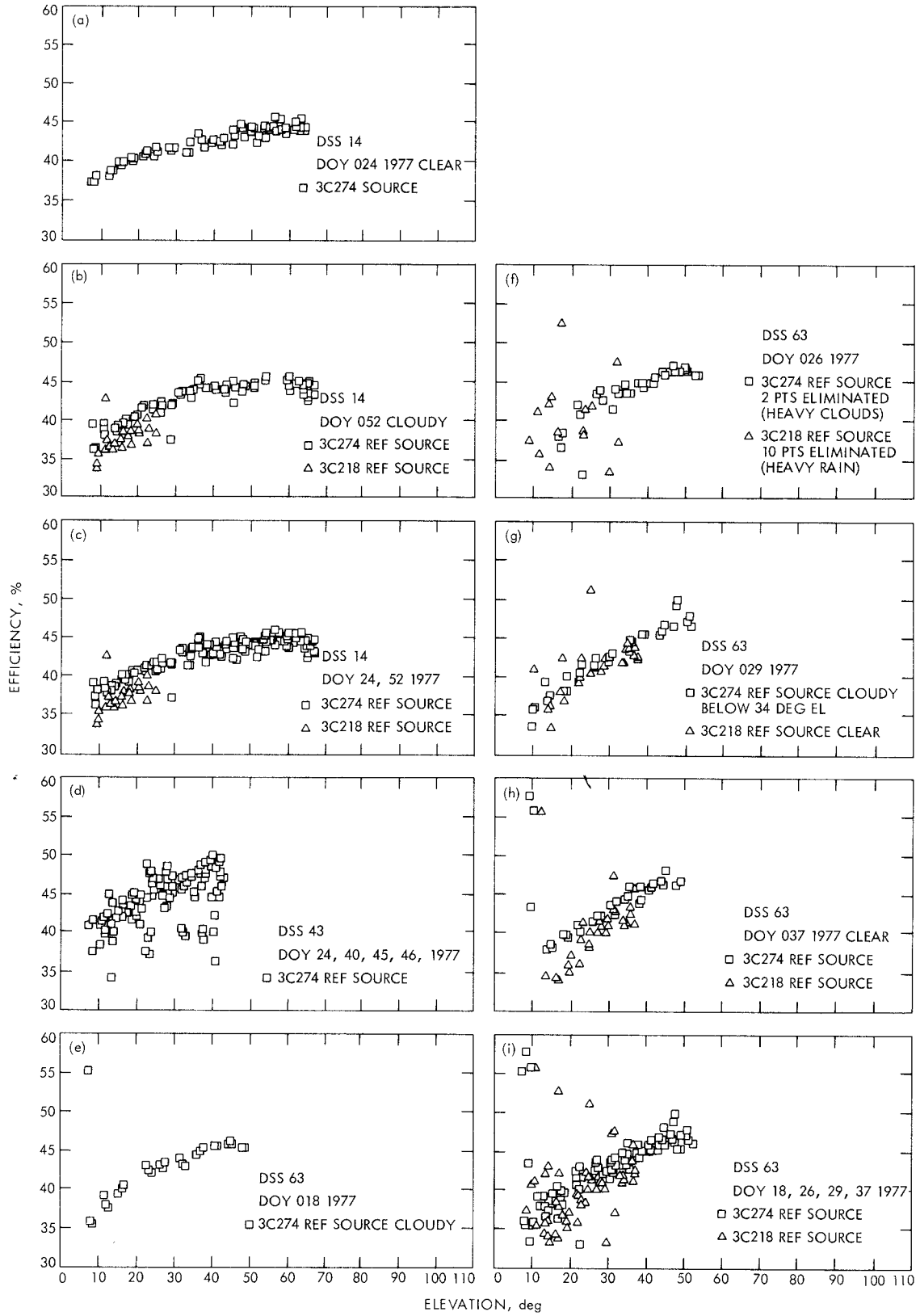

Fig. 7. Efficiency vs elevation at X-band (8415 MHz): (a) through (c) DSS 14; (d) DSS 43; (e) through (i) DSS 63

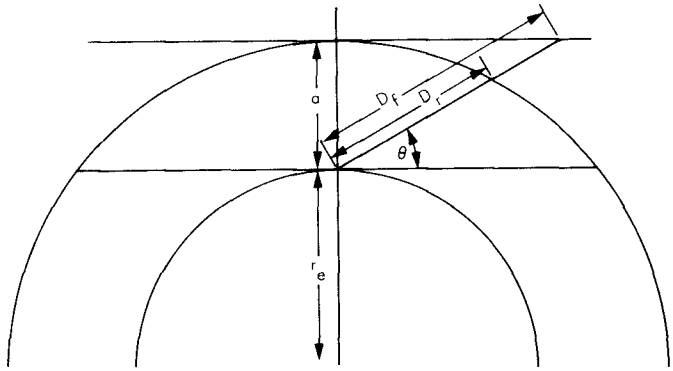

Fig. 8. Earth models

$$T_{OP} = T_R + T_{gnd} + T_{gal} + T_{atm} + T_{ar}$$

$T_R = T_M + T_F$, $T_M = 8\ K$, T_F = 1.32 K for DSS 14,
0.493 K for DSS 43,
0.936 K for DSS 63

T_{ar} = 3.88 K

T_{gnd}[a] = $29.1034\ \theta^{(-0.3673)}$ K for DSS 14

$T_{gal} = 2.7/L_\theta$ K

$$T_{atm} = \frac{(L_\theta - 1)}{L_\theta} \cdot 265 \text{ K}$$

$L_\theta = 10^{\ell_z D/10a}$, ℓ_z = 0.043 dB for clear dry weather

$D = | r \sin\theta \pm \sqrt{(r \sin\theta)^2 + 2ar + a^2} |$ for round earth

$r = a/\sin\theta$ for flat earth

θ = elevation angle in degrees

R = radio earth radio = 8500 km

a = 10 km

[a]Obtained by curvefitting measured data.

Fig. 9. A mathematical model of T_{OP}

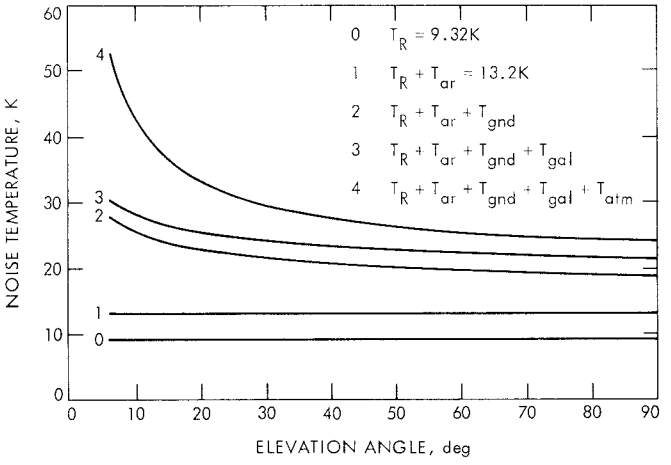

Fig. 10. Plots of the mathematical model of T_{OP} given in Fig. 8, round earth, DSS 14

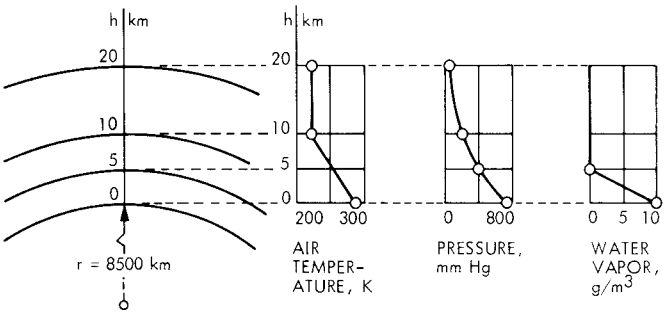

Fig. 11. Air temperature, pressure, and water vapor distribution over the earth troposphere

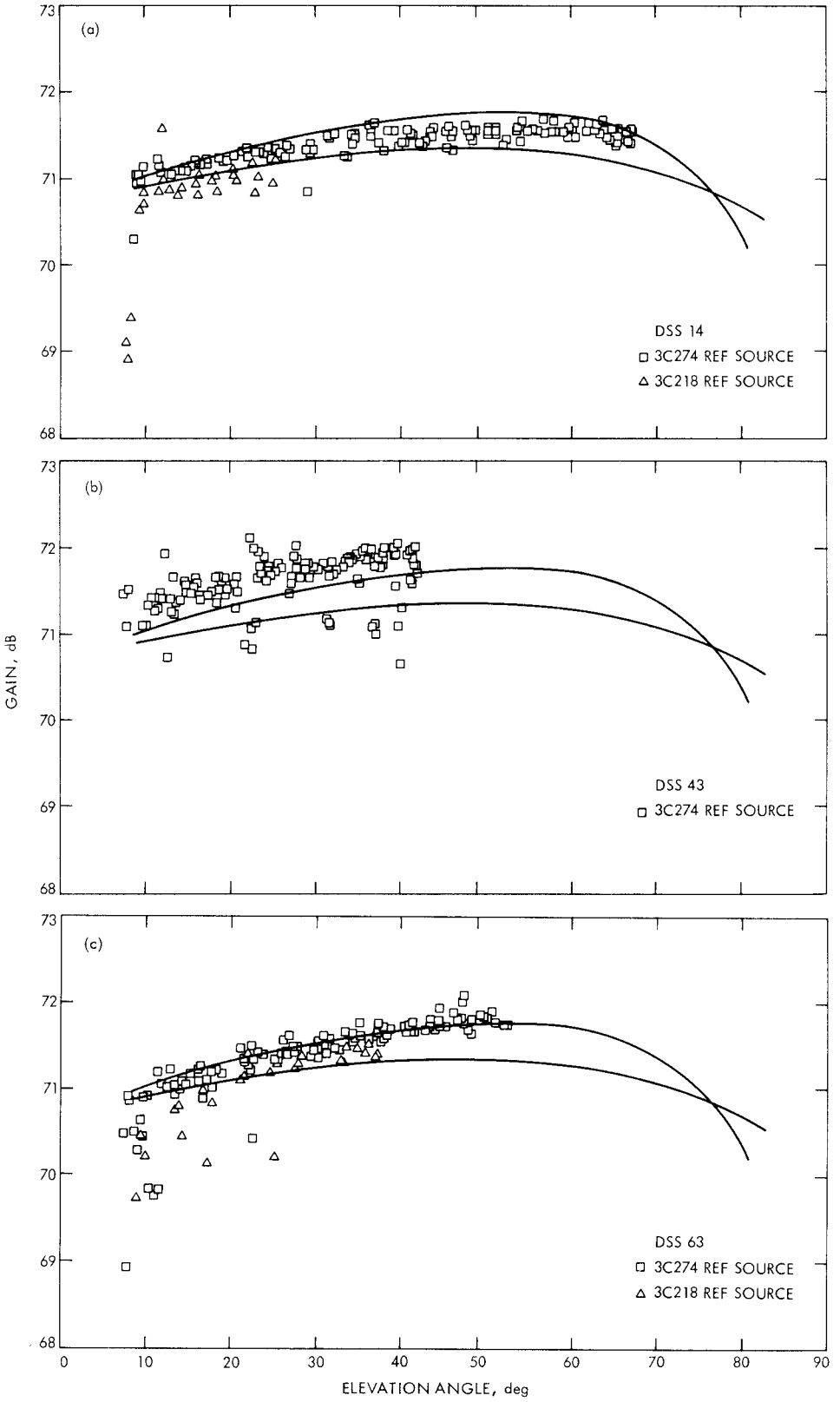

Fig. 12. Antenna gain vs elevation angle at 8415 MHz with atmospheric losses removed: (a) DSS14; (b) DSS 43; (c) DSS 63

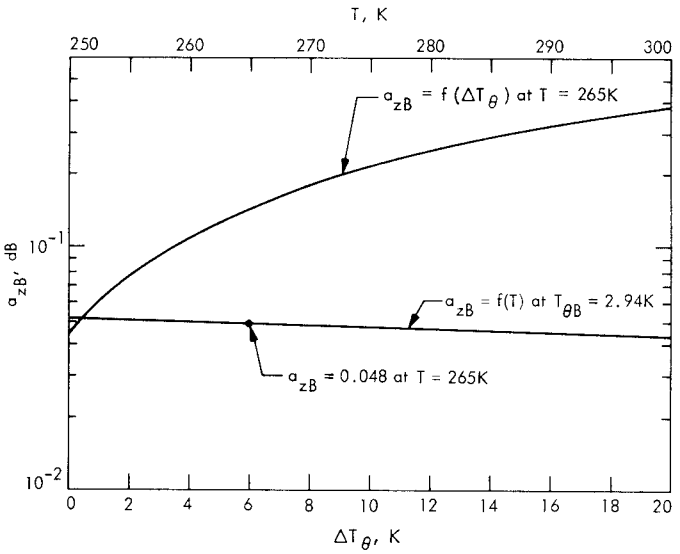

Fig 13. a_{zB} vs ΔT_θ and a_{zB} vs T

Appendix

Derivation of Observed Brightness Temperature and Star Source Flux Density

By using the concept of brightness change in an elemental volume dv (see Fig. A-1) due to emission and absorption of electromagnetic energy, the observed brightness of a radio source may be derived to be (Ref. 5):

$$B = B_s e^{-\tau} + \int_0^{\tau} e^{-(\tau - \tau')} B(T) d\tau' \qquad \text{(A-1)}$$

where

B = observed brightness, watts m^{-2} Hz^{-1} rad^{-2}

B_s = brightness of source

τ = optical depth of the medium, dimensionless

$= \tau(r) = \int_0^{r} \alpha(r')\, dr'$, dependent on the medium thickness, $\alpha(\ )$ is the absorption coefficient

T = temperature, K

For $B(T) = B_i$ = intrinsic brightness = constant, and denoting τ by τ_m for τ of a medium, Eq. (A-1) yields

$$B = B_s e^{-\tau_m} + B_i (1 - e^{-\tau_m}) \qquad \text{(A-2)}$$

With $h\nu \ll kT$ and using Maclaurin's expansion, Planck's black body radiation law

$$B(T) = 2\frac{h\nu^3}{C^2} \frac{1}{e^{h\nu/kt} - 1}$$

can be reduced to give an approximate relationship between brightness and temperature (known as the Rayleigh–Jeans law) as:

$$B(T) = 2kT/\lambda, \quad \nu = c/\lambda \qquad \text{(A-3)}$$

where

k = Boltzmann's constant (= 1.38×10^{-23} joules K^{-1})

λ = wavelength, m

ν = frequency, Hz

C = speed of light, $msec^{-1}$

h = Planck's constant (= 6.63×10^{-34} joules sec)

Thus in terms of brightness temperature, Eq. (A-2) gives (See Fig. A-1)

$$T_b = T_s e^{-\tau_m} + T_m (1 - e^{-\tau_m}) \qquad \text{(A-4)}^3$$

where

T_b = observed brightness temperature, K

T_s = source temperature, K

T_m = medium temperature, K

τ_m = optical depth of medium, dimensionless

Figure A-2 depicts a plot of Eq. (A-4) for the case $T_s > T_m$. At the optical depth of 1, T_b receives only about 67% from T_m and about 37% from T_s. A similar plot may also be obtained for the case $T_m > T_s$. When the source and medium temperatures are identical, $T_b = T_s = T_m$ and is independent of τ_m. In all cases,

$$\lim_{\tau_m \to \infty} T_b \simeq T_m$$

[3] The validity of this relationship at X-band is justifiable. For a typical $T = 298$ Kelvins, $\nu = 6.2 \times 10^{12}$ Hz (0.05-mm wave), which is 737 times larger than 8.4×10^9 Hz (3.57-cm wave) at X-band and thus the relation $h\nu \ll kT$ holds.

which states that the observed brightness temperature of an atmosphere with a very thick medium is the temperature of the medium itself.

When the temperature of the medium is not constant, we have from Eqs. (A-1) and (A-3):

$$T_b = \frac{T_s}{L} + \int_1^L \frac{T_m}{L} e^{\tau'} d\tau'$$

$$= \frac{1}{L}\left(T_s + \int_1^L T_m \, dL'\right)$$

where $L' = e^{\tau'}$ and $dL' = e^{\tau'} d\tau'$.

By defining

$$\overline{T}_m = \frac{1}{L - 1} \int_1^L T_m \, dL'$$

as a weighted average temperature from $L' = 1$ to $L' = L$, we then have

$$T_b = \frac{T_s}{L} + \frac{(L - 1)}{L} \overline{T}_m \qquad \text{(A-5)}$$

The first term on the right of Eq. (A-5) is the brightness temperature due to source. The second term is the brightness temperature due to medium, often referred to as the effective atmospheric temperature.

With a similar approach as the above, the galactic temperature effects may also be derived to be of the form

$$T_{gal} = T/L$$

Where T is the galactic temperature measured at zenith which has a nominal value of 2.7 K.

The observed flux density of a radio source can also be determined. The spectral power P or power per unit bandwidth radiated from a solid angle Ω of the sky on to an antenna of effective aperture area A_p is

$$P = (1/2) A_p \int\int B(\theta, \phi) P_n(\theta, \phi) \, d\Omega \qquad \text{(A-6)}$$

where

P = received spectral power, watts Hz^{-1}

A_p = effective aperture area of antenna, m^2

$B(\theta, \phi)$ = brightness of sky, watts m^{-2} Hz^{-1} rad^{-2}

$P_n(\theta, \phi)$ = normalized power pattern of antenna, dimensionless

$d\Omega$ = $\sin\theta \, d\theta d\phi$ = element of solid angle, rad^2

ϕ = the azimuthal angle

If the antenna is placed inside of a blackbody enclosure at a temperature T, then the brightness will be constant in all directions. According to the Rayleigh–Jeans law, its value is (see Eq. A-3):

$$B(\theta, \phi) = \frac{2kT}{\lambda^2} \qquad \text{(A-7)}$$

Since the beam area of the antenna is

$$\Omega_A = \int\int_{4\pi} P_n(\theta, \phi) \, d\Omega$$

with Eq. (A-7), Eq. (A-6) yields

$$P = \frac{kT}{\lambda^2} \cdot A_p \Omega_A = kT, \; A_p \Omega_A = \lambda^2$$

Furthermore, if the source of temperature T does not extend over the entire antenna beam area, the measured or antenna temperature T_A will be less so that

$$P = (1/2) A_p \int\int_{\Omega} B(\theta, \phi) P_n(\theta, \phi) \, d\Omega = kT_A \qquad \text{(A-8)}$$

Now when the source is observed with an antenna of power pattern $P_n(\theta_1 \phi)$, a flux density S_0 is observed to be

$$S_0 = \int\int_{\text{source}} B(\theta, \phi) P_n(\theta, \phi) \, d\Omega$$

Hence, the observed flux density of a radio source can be determined from the measured antenna temperature and its effective aperture area through the relation

$$S_0 = \frac{2kT_A}{A_p} \qquad \text{(A-9)}$$

where

S_0 = observed flux density of source, watts m^{-2} Hz^{-1}

T_A = (maximum) antenna temperature due to source, K

A_p = effective aperture area of antenna, m^2

k = Boltzmann's constant (= 1.38×10^{-23} joules K^{-1})

References

1. Freiley, A. J., "Radio Frequency Performance of DSS 14 64-m Antenna at 3.56 and 1.96 cm Wavelengths" in the *DSN Progress Report,* Technical Report 32-1526, Vol. XIX, pp. 110-115, JPL, Pasadena, California, February 15, 1974.
2. Neff, D. E., and Bathker, D. A., "DSS 14 X-Band Radar Feed Cone," *DSN Progress Report* 42-30, pp. 119-131, JPL, Pasadena, Calif., December 15, 1975.
3. Janssen, M. A., et al., "Extension of the Absolute Flux Density Scale to 22.285 GHz," *Astronomy & Astrophysics*, Vol. 33, 373-377 (1974).
4. Hogg, D. C., "Effective Antenna Temperature Due to Oxygen and Water Vapor in the Atmosphere," *J. Appl. Phys.*, Vol. 30, No. 9, September 1959.
5. Kraus, J. D., *Radio Astronomy*, McGraw-Hill, 1966.

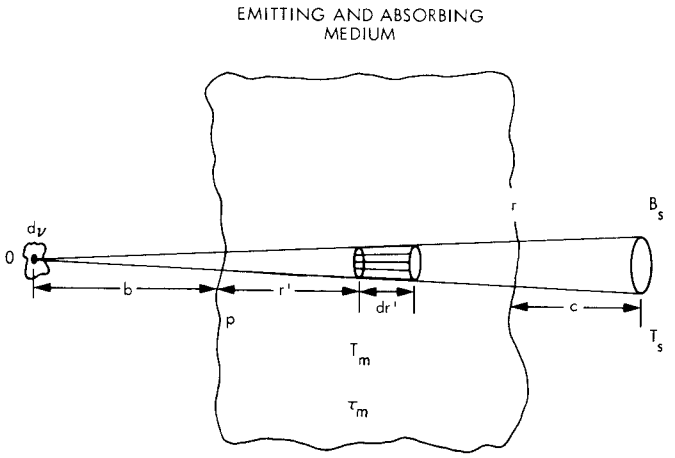

Fig. A-1. Source of brightness B_s (or brightness temperature T_s) observed through an intervening medium of temperature T_m and optical depth τ_m

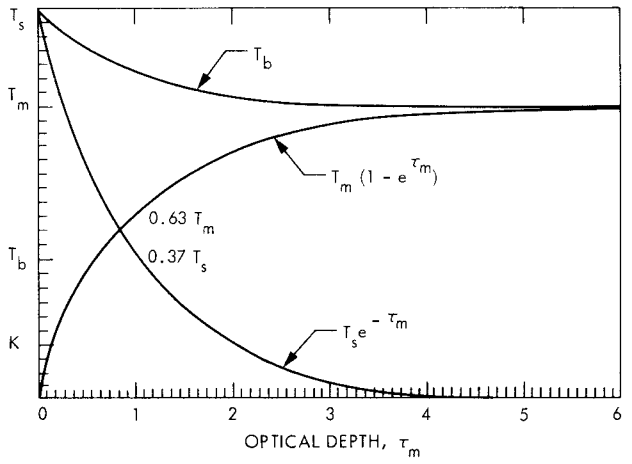

Fig. A-2. Variation of brightness temperature due to emission, absorption, and both as a function of optical depth, τ_m; $T_s > T_m$